

A Study of Atmospheric Aerosols in The Bahamas Using Camera Lidar and Star Photometry Techniques

Amin S. Kabir  <https://orcid.org/0000-0002-5757-7498>

University of The Bahamas

Nimmi C. Sharma  <https://orcid.org/0000-0002-7439-7114>

Central Connecticut State University

Edward Knowles  <https://orcid.org/0009-0007-1617-7993>

University of The Bahamas

Seth Gagnon  <https://orcid.org/0000-0003-0902-1935>

Central Connecticut State University

Justin Fagnoni  <https://orcid.org/0009-0009-4180-0091>

Central Connecticut State University

John E. Barnes  <https://orcid.org/0000-0002-4953-210X>

NOAA/ESRL/Global Monitoring Laboratory, Boulder, CO

Abstract

Aerosols, the tiny suspended particles in the atmosphere, are a widely studied topic around the world due to their effects on the Earth's radiation budget, climate change, and human health. Knowledge of the spatial and temporal distribution of aerosols is essential to assess air pollution and predict potential climate change. This study measured aerosol optical depth (AOD) and altitude-dependent aerosol extinctions in Nassau, The Bahamas simultaneously using a camera-based imaging lidar (CLidar). The bistatic geometry of the setup which consisted of a wide-angle lens fitted to a charge-coupled device (CCD) camera, allowed for the measurement of extinctions at all altitudes at once without requiring expensive timing electronics common to lidars. A case study was conducted on November 5, 2018. The top of the boundary layer beyond which aerosol extinction was nearly zero was detected at ~ three km above sea level. Due to the excellent resolution of the CLidar at lower altitudes, variations of aerosol concentrations within the boundary layer are efficiently detected. Optical depth was measured using the same CLidar camera at the same time, utilising star photometry, and was found to be 0.043 ± 0.040 . The value falls within the range of assumed values of AOD near the regions obtained from the Moderate Resolution Imaging Spectroradiometer (MODIS) Aqua satellite.

DOI: <https://doi.org/10.15362/ijbs.v29i1.519>

Introduction

Aerosols are tiny suspended solid and liquid particles in the atmosphere that can originate naturally (e.g. windblown dust, sea salt, smoke from wildfires, volcanic ash) or from human activities (e.g. pollution from factory and vehicle emissions, waste disposition in landfills). Aerosols play a key role in the cooling and warming of the Earth's surface, cloud formation, and precipitation patterns (Charlson et al., 1992; Fiore et al., 2012; Kaufman et al., 2002; Leung & Gustafson, 2005). Aerosol characteristics and concentrations may be used to predict potential climate change (Leung & Gustafson, 2005; Myhre et al., 2013). Local and regional air quality and their effects on human health are also directly influenced by aerosols (Kinney, 2008; Levy et al., 2013). Due to their decisive role in global and regional climate change and on air quality, aerosols are studied extensively around the world. However, the distribution of aerosols and their properties vary greatly both over time and location, making it challenging for in-situ aerosol profiling, specifically temporal and spatial distributions (Mao et al., 2014).

Optical properties of aerosols like extinction, aerosol optical depth (AOD), mass scattering coefficients, and angstrom exponents can reveal the quantity and characteristics of the aerosols and, hence, their effects on the environment and climate change (Liu et al., 2014). Aerosol extinction is a measure of solar and terrestrial radiation loss per unit length travelling through atmospheric aerosols. AOD represents aerosol extinctions summed through the entire vertical column of the atmosphere, however, it is often dominated by the atmospheric boundary layer. Traditional monostatic lidar systems are capable of measuring altitude-dependent aerosol extinction with excellent resolution at higher altitudes but suffer an overlap effect

due to the collocated detector and transmitter at lower altitudes (Welton & Campbell, 2002). The CLidar does not have this challenge, however, and accurately measures aerosol extinction in high resolution all the way to the ground. Aircraft and balloon-borne devices can also measure aerosol properties but are not as suitable for frequent monitoring (Baumgardner et al., 2011) due to cost and logistics. AERONET (Aerosol Robotic Network) uses ground-based radiometers to measure AOD but is not available in The Bahamas (Goddard Space Flight Center, 2023). NASA's Moderate Resolution Imaging Spectroradiometer (MODIS) Aqua satellite covers most of the regions on Earth to calculate AOD, but does not monitor New Providence Island and nearby regions as frequently as desired (National Aeronautics and Space Administration, 2023). Therefore, an inexpensive charge-coupled device (CCD) camera-based bistatic imaging lidar system was employed in this study to simultaneously measure nocturnal aerosol scattered light and optical depth (Barnes et al., 2007; Barnes & Sharma, 2012). Unlike traditional lidar, the bistatic system uses a CCD camera as a detector which is fitted with a wide-angle lens and is placed at a distance from the laser transmitter. This geometry allows measurements to be taken at all scattering altitudes at once without requiring scanning at various angles to capture altitude-dependent scatterings. High altitude resolution in the near-ground levels (< 1 m) enables the system to detect air pollution from local sources (Kabir et al., 2018). Stars captured in the CCD camera simultaneously with the image of the laser are used to calculate optical depth by employing star photometry (Barnes et al., 2016). Due to the simultaneous measurements of aerosol scatter and AOD at the same location and time using the same CCD camera, the parameters can be linked to each other. The

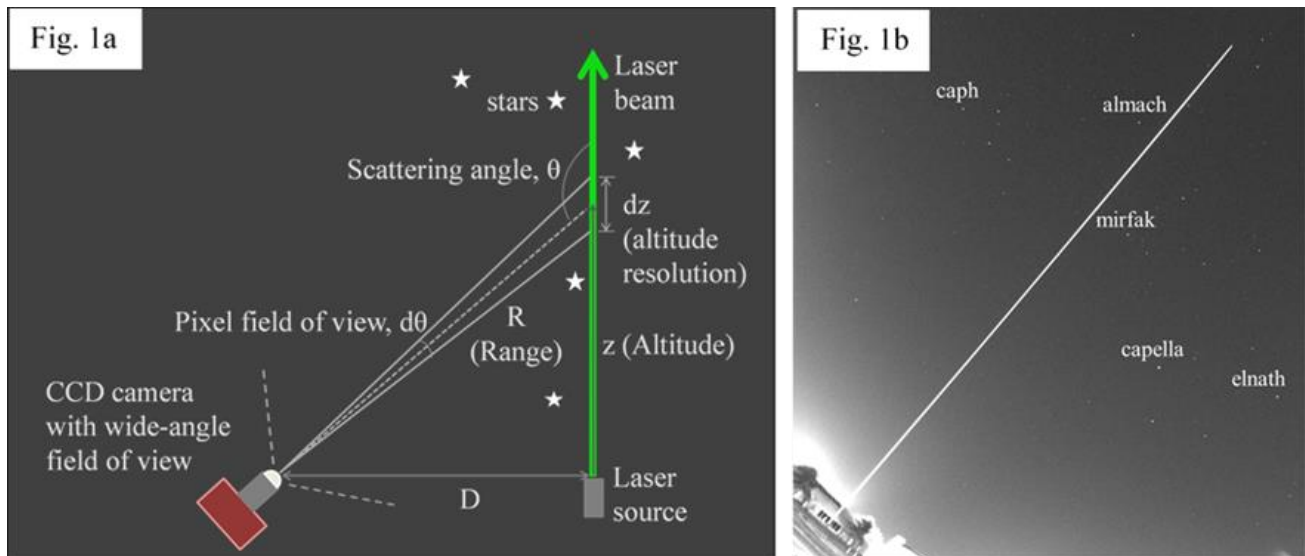
measurements can also be compared with MODIS Aqua satellite AOD data.

Method for aerosol extinction measurements

CLidar geometry is shown in Figure 1a. A ground-based continuous wave laser at 532 nm wavelength was set to transmit vertically into the atmosphere, and a CCD camera was placed a distance, D (~ 92 m), away from the laser beam. An interference filter at 532 nm was inserted between the camera and lens to

allow scattered light at 532 nm to enter the camera while blocking background light at other wavelengths. The camera was fitted with a wide-angle lens to capture the entire laser beam from ground to zenith at once, without the need for scanning. Each section of the vertical laser beam corresponded to a scattering altitude. Unlike monostatic lidar (where a pulsed laser is used), the scattering altitudes were determined simply by CLidar geometry without requiring expensive time-gating electronics.

Figure 1a Setup of the CLidar. **1b** CCD Image of the Laser from Ground to Zenith and the Stars



Note: The laser image was analysed to calculate aerosol extinction and the stars were used to calculate optical depth.

Due to the constant angular field of view ($d\theta = 0.03^\circ / \text{pixel}$) of the lens captured dz (the length of the laser beam at altitude z) is smaller at the ground levels compared to higher altitudes. Therefore, CLidar enables excellent resolution at ground levels and in the boundary layer compared to traditional lidars, which suffer low resolution and overlap problems at ground levels due to the co-located laser transmitter and detector.

Figure 1b shows the image of the laser beam from ground to zenith along the diagonal of the CCD chip and provides an example of how a raw data file appears. The scattered light signal is calculated pixel by pixel along the beam. The CCD image of the laser beam, seen in the figure during a cloud-free night, contains both molecular (composed of air molecules) and aerosol single-angle scattering. A model of molecular scattering

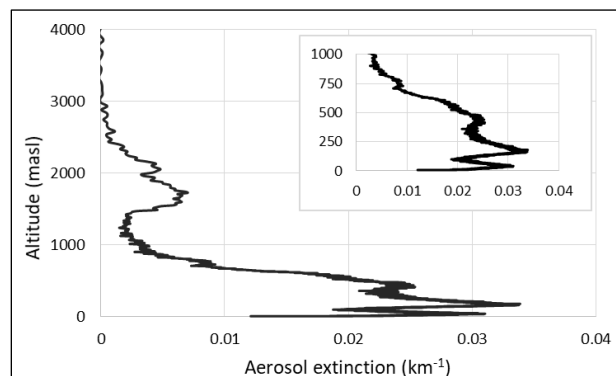
constructed using Nassau radiosonde data and the NASA MSIS-E-90 atmospheric model at higher altitudes was subtracted from the signal to retrieve the aerosol portion (University of Wyoming, n.d.; “NRLMSIS Atmosphere Model”, n.d.). It should be noted that lidar aerosol analysis usually requires an assumption of the ratio of extinction to a 180-degree backscattered light in order to calculate extinction and AOD. CLidar requires the additional assumption of the form of the ratio between 90–180 degrees. This dependence of the amount of scattered light to the scattering angle is called the aerosol phase function (APF). Very few APFs are measured, and when they are, most are calculated from assumed or measured aerosol properties such as particle size distribution and complex index of refraction. In this analysis, the Polluted Continental aerosol phase function assumed by CALIPSO satellite measurements is obtained from NASA’s Atmospheric Science Data Center and is used to calculate total aerosol scatter. Finally, since the APF accounts for total scatter and not extinction, a single scattering albedo obtained from the CALIPSO database is also assumed. The single scattering albedo accounts for aerosol absorption (aerosol extinction = total scatter + absorption).

Experimental results of extinction measurements

The experiments were conducted at the sports field of University of The Bahamas, Nassau, New Providence, located about 2 km from the shoreline and at an altitude of a few meters above sea level. The island is situated in the Atlantic Ocean at 25.06° N and -77.35° W. Images were captured during local times, 9:15 p.m. to 11:05 p.m., on November 5, 2018. Several images were captured using 30 s and 120 s exposure times. Figure 2 illustrates CLidar aerosol extinction as a function of altitude in meters above sea level

(masl) at local time 10:59 p.m. Due to excellent resolution at lower altitudes, the CLidar instrument resolves variations of aerosol concentrations near ground levels where traditional monostatic lidar systems may suffer from overlap issues. For example, the CLidar observed a thin aerosol layer where the extinction increased from ground level to 40 m altitude, reaching a value of 0.31 km⁻¹ and then dropping off. The maximum extinction of 0.34 km⁻¹ was detected at ~180 m altitude. The measurements reveal the dropoff of extinction to very low values, at 2.6 km above sea level, indicating the top of the atmospheric boundary layer beyond which aerosol concentrations are often nearly zero.

Figure 2 Aerosol Extinction as a Function of Altitude Above Sea Level obtained by Analysing the CLidar Image of the Laser



Note: Inset shows the extinctions from ground level to 1 km to demonstrate the efficacy of CLidar to capture the extinction variations at lower altitudes.

The uncertainty of the extinction calculation for CLidar can be up to 200%, most of which arises from the selection of the assumed phase function (Barnes et al., 2007; Kabir, 2021). If available at the experimental site or nearby, AERONET phase functions can be utilised in the analysis to reduce the uncertainty of extinction. Although not a direct measurement of the APF, the AERONET Sun photometer can scan a range of angles away from the sun and retrieve an

average APF. While there are some AERONET sites in Miami and Cuba, those locations are too far from The Bahamas and may not be representative of Nassau's aerosol phase functions (Goddard Space Flight Center, 2023). Further, since AERONET ground-based radiometers measure phase functions only at the ground level, while the scattering depends on the aerosol types at different altitudes, the AERONET phase functions will still lead to significant uncertainty in extinction calculations. Using two cameras at two different distances from the laser can provide altitude-dependent aerosol phase functions and significantly reduce the error in the extinction calculation (Lian et al., 2019). Currently, we are working on the two-camera CLidar technique to calculate extinction. The CLidar instrument demonstrates the potential for linking remote sensing and in-situ environmental characterisation for detecting air pollution or monitoring and assessing seasonal atmospheric features to help illuminate characteristics of local atmospheric structure (Kabir et al., 2022; Kabir et al., 2020).

Method for aerosol optical depth measurements

The stars imaged at the same location, time, and through the same interference filter (at 532 nm) as the laser beam are used in the star photometry method to calculate AOD simultaneously with aerosol profiles (Barnes et al., 2016). CCD exposure time of 30 s was used to capture the image of the stars. A two-star method depicted in Figure 3 is employed to calculate AOD, which does not require a calibration of the instrument such as a Langley plot (Leiterer et al., 1995).

The extraterrestrial spectral energy density of the stars (U_0) was obtained by the Pulkovo spectroscopic catalog (Alekseeva et al., 1996). Elevation angles (h) were determined by the latitude and longitude of the observer's location and the right ascension and declination of the stars (National Astronomical Observatory of Japan, 1994). Selecting the exposure time to capture the image of the stars was critical. Too small of an exposure time would not have provided enough intensity of the stars at the CCD to work with. For large exposure times, stars will change their elevations, resulting in elongated images at the CCD and, hence, would have yielded errors in intensity calculations. Equations used to calculate optical depth using star photometry are presented in Table 1. Air masses (F) were calculated by substituting the elevation angles of the stars in Equation 1. The intensity of the stars (U) imaged on the CCD detector was summed using a two-dimensional Gaussian fit (Equation 2) to the pixel intensity.

Figure 3 Star Photometry using the Two-Star Technique to Calculate AOD

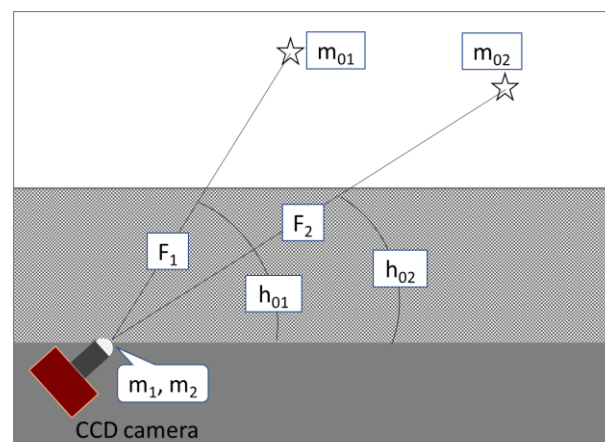


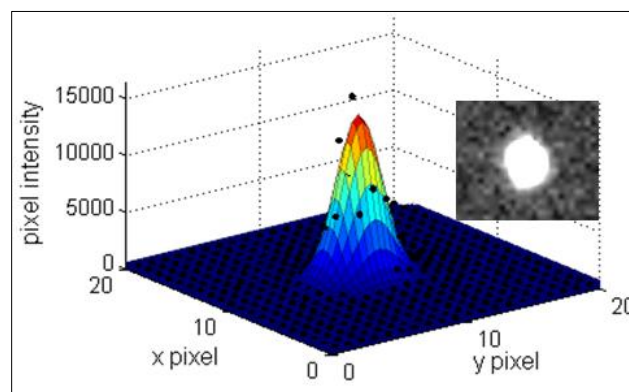
Table 1 Equations for Two-Star Photometry

$F = 1/(\sin h)$	(1)
$f(x, y) = A * \text{Exp}(-((x - b_1)^2/(2 * \sigma_1^2) + (y - b_2)^2/(2 * \sigma_2^2))) + d$	(2)
Star intensity, U at the detector = $2 * \pi * A * \sigma_1 * \sigma_2$	(3)
$m_1 - m_2 = -2.5 \log_{10}(U_1/U_2)$	(4)
$m_{01} - m_{02} = -2.5 \log_{10}(U_{01}/U_{02})$	(5)
$\alpha = ((m_1 - m_2) - (m_{01} - m_{02})) / (F_1 - F_2)$	(6)
$\delta_T = 1.086/\alpha$	(7)
$\delta_{Ray} = (P/P_0) * 0.00879 * \lambda^{-4.09}$	(8)

The stars used are shown in Figure 1b. In Equation 2, A is the peak amplitude; b_1 and b_2 are the position of the intensity peaks on the x and y grid; σ_1 and σ_2 are the width of the Gaussians along the x and y axes, and d is the constant background. Star intensities U at the CCD camera were then calculated using Equation 3 which is simply the area under the Gaussian curve. The best fit can be obtained for nearly circular images of the stars for smaller exposure times. Figure 4 illustrates the fitting of the CCD pixel intensity of the star Capella using the 2-dimensional (2D) Gaussian function. The difference in terrestrial brightness at the observer location ($m_1 - m_2$) and the difference in extraterrestrial brightness ($m_{01} - m_{02}$) were calculated using Equations 4 and 5. Total atmospheric thickness, δ_T includes optical thickness for pure gaseous molecules (δ_{Ray}), aerosols (δ_{Aer}), water vapor (δ_{wv}), nitrogen dioxide (δ_{NO_2}) and ozone (δ_{O_3}) and is determined using Equation 6 and Equation 7. To obtain AOD, the contributions from other components needed to be subtracted. Rayleigh optical thickness for pure gaseous atmosphere (δ_{Ray}) was obtained using Equation 8 where P (1018 hPa) is the relevant

air pressure at the site during the experiment; P_0 is 1013 hPa and λ is 0.532 μm . Scattering and absorption due to water vapor at 532 nm was negligible, and, thus, contributions for δ_{wv} can be neglected (Leiterer et al., 1995). Instrumentation to measure optical thickness for O_3 and NO_2 was not available, but their contributions would have been small. Strictly speaking, our calculated optical thickness by star photometry was expected to be the upper limit for aerosol. Future work will use model estimates to account for O_3 and NO_2 .

Figure 4 Fitting of the Pixel Intensity of Capella using 2-Dimensional Gaussian Function in Matlab



Note: Inset shows the CCD image of the star Capella.

Table 2 Stars used to Calculate Optical Depth (Aerosols + Ozone + Nitrogen Dioxide)

Stars	Elevation angle, h ($^{\circ}$)	Energy flux density at 532 nm, U_0 ($W/m^2.m$)	Pixel intensity, U (Area under 2D Gaussian fit)	R^2 of the Gaussian fits
Almach (HR603)	72.4098	0.005114	25720	0.96
Mirfak (HR1017)	59.1385	0.007125	34447	0.90
Caph (HR21)	51.5500	0.00463	20661	0.93
Capella (HR1708)	43.9838	0.03487	152781	0.96
Elnath (HR1791)	42.0205	0.00853	31772	0.92

Note: The experimental site was University of The Bahamas, Oakes Field Campus, Nassau on November 5, 2018, at local time 22:59.

Experimental results of optical depth measurements

Optical depth (aerosols + ozone + nitrogen dioxide) for four different pairs were calculated using five stars presented in Tables 2 and 3. Pairs of stars were chosen such that the difference of the elevation angles for each pair was more than 15° to ensure a large air mass difference. Smaller air mass difference yields large errors in the calculation (Barnes et al., 2016). Optical depth calculation also strongly depends on

the calculated intensity of the stars, using the 2D Gaussian model. For example, a 10% variation of the calculated intensity can lead to a deviation of AOD by 100%. The coefficient of determination (R^2) for the model fit for all star intensities is above 0.9 and, thus, the error in AOD calculation is less than 100%. The calculated average optical depth using the two-star photometry method is 0.043 ± 0.040 at local time 22:59 on November 5, 2018, at University of The Bahamas Oakes Field Campus in Nassau.

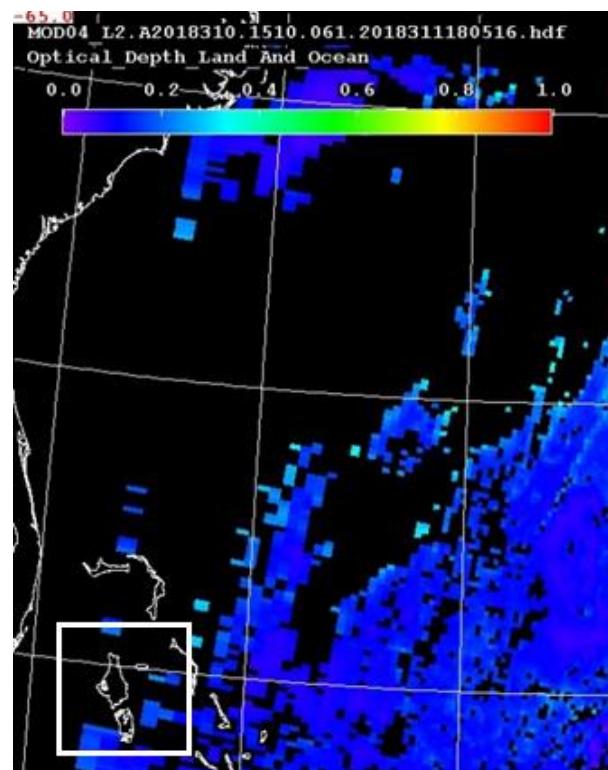
Table 3 Calculation of Average Optical Depth

Pairs of stars	$m_1 - m_2$	$m_{01} - m_{02}$	$F_1 - F_2$	α	δ_T	(Avg. $\delta_T - \delta_{Ray}$)
Mirfak, Capella (18 $^{\circ}$ deviation)	2.17	2.19	-0.59	0.03	0.03	0.043 \pm 0.040
Mirfak, Elnath (26 $^{\circ}$ deviation)	0.47	0.66	-0.84	0.23	0.22	
Almach, Capella (23 $^{\circ}$ deviation)	1.93	2.08	-0.72	0.21	0.19	
Almach, Caph (16 $^{\circ}$. deviation)	0.32	0.36	-0.20	0.22	0.20	

The calculated optical depth (aerosol + ozone + nitrogen dioxide) by star photometry method can help constrain the CLidar extinction measurements and the assumed APF used. The altitude-dependent extinction profile in Figure 2 is integrated along the vertical column from the ground to the top of the atmospheric boundary layer (~3 km) to obtain an AOD of 0.023. The AOD would be higher if the entirety of the atmosphere above three km was included. A reasonable AOD estimate for the stratospheric aerosol layer is 0.006 ± 0.001 . The basis of this estimate is results obtained from 11 observations from 2018/10 through 2018/12 from the NOAA Mauna Loa Observatory lidar in Hawaii (Barnes & Hofmann, 2001), which is located at a similar latitude as The Bahamas. The stratospheric AOD is already included in the star photometer measurement of 0.043 since it measures the entire atmosphere. There would also be a free troposphere contribution between the boundary layer and the stratosphere which we assume is near zero in CLidar analysis but could account for the difference in AOD measured by star photometry and integrated CLidar extinction (0.043 vs $0.023 + (?) + 0.006$). Note that the difference can also be attributed to the assumed aerosol phase function in the CLidar extinction analysis not accurately representing the observed aerosol, which illustrates the power of having both the CLidar extinction and the star photometer AOD. We also examined MODIS AQUA satellite measurements to retrieve AOD (at 550 nm radiation wavelength) near our experimental region (Levy et al., 2015). As seen in Figure 5, satellite AOD data are

available for nearby Nassau regions but not exactly over Nassau on November 5, 2018. From this figure, AOD at the experimental site is assumed to be in the range of 0.01-0.15. Optical depth, calculated by star photometry and by integrated CLidar extinctions, falls within this range. According to NASA Earth Observatory an AOD value of < 0.01 corresponds to extremely clean air and > 0.4 corresponds to very hazy conditions. AOD ~ 0.1 is considered clean air.

Figure 5 MODIS Aerosol Optical Depth near Nassau on November 5, 2018



Note: The white square box in the image highlights the MODIS AOD near Nassau.

Conclusion

In conclusion, aerosol optical depth by star photometry and altitude-dependent aerosol extinctions in Nassau, The Bahamas were measured simultaneously using a CLidar setup. The system is simple, inexpensive, and portable. The excellent altitude resolution of CLidar at lower altitudes makes it an efficient tool for profiling boundary layer aerosols. Since optical depth is measured simultaneously with CLidar aerosol extinction by using star photometry it can constrain the optical depth calculated from integrated CLidar extinction profiles. The measured optical depth of 0.043 ± 0.040 using star photometry on November 5, 2018, falls within the range of AOD values assumed from MODIS Aqua satellite

measurements near the Nassau region. The work is in progress to improve the accuracy of the extinction measurements by using a two-camera CLidar system which is capable of also constraining the aerosol phase function. In addition, two cameras will be used at two different orientations to capture more stars at once to ensure that a minimum of 20 pairs of stars can be used to find AOD with greater accuracy. CLidar and star photometry experiments will be conducted seasonally and at other islands of The Bahamas to study aerosols and their effects in the region. In addition, the number and mass density of size-dependent aerosols will be measured from ground-based air quality devices and will be compared with CLidar measurements.

Acknowledgments

This work was supported by an internal research grant from University of The Bahamas. The experiment was conducted at University of The Bahamas, Oakes Field Campus in Nassau, New Providence Island on November 5, 2018.

References

- Alekseeva, G., Arkharov, A., Galkin, V., Hagen-Thorn, E., Nikanorova, I., Novikov, V., Novopashenny, V., Pakhomov, V., Ruban, E., & Shchegol, D. (1996). The Pulkovo spectrophotometry catalog of bright stars in the range from 320 to 1080 nm. *Open Astronomy*, 5(4), 603-838. <https://doi.org/10.1515/astro-1996-0401>
- Barnes, J. E., & Hofmann, D. J. (2001). Variability in the stratospheric background aerosol over Mauna Loa Observatory. *Geophysical Research Letters*, 28(15), 2895-2898. <https://doi.org/10.1029/2001GL013127>
- Barnes, J. E., & Sharma, N. C. (2012). An inexpensive active optical remote sensing instrument for assessing aerosol distributions. *Journal of the Air & Waste Management Association*, 62(2), 198-203. <https://doi.org/10.1080/10473289.2011.639927>
- Barnes, J. E., Pipes, R., & Sharma, N. C. (2016). Measuring aerosol optical depth (AOD) and aerosol profiles simultaneously with a camera lidar. *EPJ Web of Conferences*, 119, 02007. <https://doi.org/10.1051/epjconf/201611902007>

- Barnes, J. E., Sharma, N. C. P., & Kaplan, T. B. (2007). Atmospheric aerosol profiling with a bistatic imaging lidar system. *Applied Optics*, *46*(15), 2922–2929. <https://doi.org/10.1364/AO.46.002922>
- Baumgardner, D., Brenguier, J. L., Bucholtz, A., Coe, H., DeMott, P., Garrett, T. J., Gayet, J. F., Hermann, M., Heymsfield, A., Korolev, A., Krämer, M., Petzold, A., Strapp, M., Pilewskie, P., Taylor, J., Twohy, C., Wendisch, M., Bachalo, W., & Chuang, P. (2011). Airborne instruments to measure atmospheric aerosol particles, clouds and radiation: A cook's tour of mature and emerging technology. *Atmospheric Research*, *102*(1-2), 10–29. <https://doi.org/10.1016/j.atmosres.2011.06.021>
- Charlson, R. J., Schwartz, S. E., Hales, J. M., Cess, R. D., Coakley, J. A., Jr., Hansen, J. E., & Hofmann, D. J. (1992). Climate forcing by anthropogenic aerosols. *Science*, *255*(5043), 423–430. <https://doi.org/10.1126/science.255.5043.423>
- Fiore, A. M., Naik, V., Spracklen, D. V., Steiner, A., Unger, N., Prather, M., Bergmann, D., Cameron-Smith, P. J., Cionni, I., Collins, W. J., Dalsøren, S., Eyring, V., Folberth, G. A., Ginoux, P., Horowitz, L. W., Josse, B., Lamarque, J. F., MacKenzie, I. A., Nagashima, T., ... Zengu, G. (2012). Global air quality and climate. *Chemical Society Reviews*, *41*(19), 6663–6683. <https://pubs.rsc.org/en/content/articlelanding/2012/cs/c2cs35095e>
- Goddard Space Flight Center. (2023). *AERONET: Aerosol Robotic Network*. <https://aeronet.gsfc.nasa.gov/>
- Kabir, A. S., Sharma, N. C., Barnes, J. E., Butt, J., & Bridgewater, M. (2018, May 10). Using a bistatic camera lidar to profile aerosols influenced by a local source of pollution. *Laser Radar Technology and Applications XXIII*, *10636*, 126-132. <https://doi.org/10.1117/12.2303544>
- Kabir, A. S., Sharma, N. C., Gagnon, S., Alcantara-Silva, M., Odhiambo, G., & Barnes, J. E. (2022, July 11-15). *Detection of aerosols in The Bahamas during Saharan dust transport times with a laser and a CCD imager*. Optics and Photonics for Sensing the Environment 2022, Vancouver, British Columbia. <https://doi.org/10.1364/ES.2022.EM2D.5>
- Kabir, A. S., Sharma, N. C., Knowles, E., Bain, C., Gagnon, S., Fagnoni, J., & Barnes, J. E. (2020, June 22-26). *Profiling boundary layer aerosols in The Bahamas at various time of year using a camera-based imaging Lidar*. Optics and Photonics for Sensing the Environment 2020, Washington, DC. <https://doi.org/10.1364/ES.2020.ETu4E.5>
- Kabir, A., Sharma, N., Barnes, J. E., Urbanczyk, A., Fagnoni, J., Gagnon, S., Alcantara-Silva, M., & Knowles, E. (2021, July 11-16). *Dependence of aerosol extinction measurements using a camera based lidar on various aerosol phase functions*. IEEE International Geoscience and Remote Sensing Symposium IGARSS, Brussels, Belgium. <https://doi.org/10.1109/IGARSS47720.2021.9554695>
- Kaufman, Y. J., Tanré, D., & Boucher, O. (2002). A satellite view of aerosols in the climate system. *Nature*, *419*(6903), 215–223. <https://doi.org/10.1038/nature01091>

- Kinney, P. L. (2008). Climate change, air quality, and human health. *American Journal of Preventative Medicine*, 35(5), 459–467.
<https://doi.org/10.1016/j.amepre.2008.08.025>
- Leiterer, U., Naebert, A., Naebert, T., & Alekseeva, G. (1995). A new star photometer developed for spectral aerosol optical thickness measurements. *Contributions to Atmospheric Physics*, 68(2), 133–142.
<https://www.osti.gov/etdeweb/biblio/178652>
- Leung, L. R., & Gustafson, W. I., Jr. (2005). Potential regional climate change and implications to US air quality. *Geophysical Research Letters*, 32(16), L16711.
<https://doi.org/10.1029/2005GL022911>
- Levy, H., Horowitz, L. W., Schwarzkopf, M. D., Ming, Y., Golaz, J. C., Naik, V., & Ramaswamy, V. (2013). The roles of aerosol direct and indirect effects in past and future climate change. *Journal of Geophysical Research: Atmospheres*, 118(10), 4521–4532.
<https://doi.org/10.1002/jgrd.50192>
- Levy, R., & Hsu, C. (2015, February 6). MODIS Atmosphere L2 Aerosol Product. NASA MODIS Adaptive Processing System, Goddard Space Flight Center, USA.
https://doi.org/10.5067/MODIS/MOD04_L2.006
- Lian, S., Bian, Y., Zhao, G., Li, W., & Zhao, C. (2019). Dual CCD detection method to retrieve aerosol extinction coefficient profile. *Optics Express*, 27(20), A1529–A1543.
<https://doi.org/10.1364/oe.27.0a1529>
- Liu, Y., Jia, R., Dai, T., Xie, Y., & Shi, G. (2014). A review of aerosol optical properties and radiative effects. *Journal of Meteorological Research*, 28(6), 1003–1028.
<https://doi.org/10.1007/s13351-014-4045-z>
- Mao, K. B., Ma, Y., Xia, L., Chen, W. Y., Shen, X. Y., He, T. J., & Xu, T. R. (2014). Global aerosol change in the last decade: An analysis based on MODIS data. *Atmospheric Environment*, 94, 680–686.
<https://doi.org/10.1016/j.atmosenv.2014.04.053>
- Myhre, G., Myhre, C. E. L., Samset, B. H., & Storelvmo, T. (2013). Aerosols and their relation to global climate and climate sensitivity. *Nature Education Knowledge*, 4(5), 7.
<https://www.nature.com/scitable/knowledge/library/aerosols-and-their-relation-to-global-climate-102215345/>
- National Aeronautics and Space Administration. (2023). *MODIS: Moderate Resolution Imaging Spectroradiometer*.
<https://modis.gsfc.nasa.gov/about/>
- National Astronomical Observatory of Japan. (1994). *Altitude/azimuth of stars*
https://eco.mtk.nao.ac.jp/cgi-bin/koyomi/cande/horizontal_rhip_en.cgi
- NRLMSIS Atmosphere Model*. (n.d.).
<https://kauai.ccmc.gsfc.nasa.gov/instrun/n/nrlmsis/>
- University of Wyoming. College of Engineering. Department of Atmospheric Science. (n.d.). *Soundings*.
<http://weather.uwyo.edu/upperair/sounding.html>

Welton, E. J., & Campbell, J. R. (2002).
Micropulse lidar signals: Uncertainty
analysis, *Journal of Atmospheric and
Oceanic Technology*, 19(12), 2089–2094.
[https://doi.org/10.1175/1520-
0426\(2002\)019%3C2089:MLSUA%3E2.
0.CO;2](https://doi.org/10.1175/1520-0426(2002)019%3C2089:MLSUA%3E2.0.CO;2)